Rapid Calibration of Operational and Research Meteorological Satellite Imagers. Part II: Comparison of Infrared Channels

PATRICK MINNIS AND LOUIS NGUYEN

Atmospheric Sciences, NASA Langley Research Center, Hampton, Virginia

DAVID R. DOELLING

Analytical Services and Materials, Inc., Hampton, Virginia

DAVID F. YOUNG

Atmospheric Sciences, NASA Langley Research Center, Hampton, Virginia

WALTER F. MILLER

Science Applications International Corporation, Hampton, Virginia

DAVID P. KRATZ

Atmospheric Sciences, NASA Langley Research Center, Hampton, Virginia

(Manuscript received 22 January 2002, in final form 11 March 2002)

ABSTRACT

To establish a more reliable reference instrument for calibration normalization, this paper examines the differences between the various thermal infrared imager channels on a set of research and operational satellites. Mean brightness temperatures from the Visible Infrared Scanner (VIRS) on the *Tropical Rainfall Measuring Mission* (*TRMM*) satellite and the second Along-Track Scanning Radiometer (ATSR-2) on the second *European Remote Sensing Satellite* (*ERS-2*) are correlated with matched data from the eighth *Geostationary Operational Environmental Satellite* (*GOES-8*), the fifth *Geostationary Meteorological Satellite* (*GMS-5*), and with each other. VIRS data are also correlated with the *Terra* satellite's Moderate Resolution Imaging Spectroradiometer (MODIS) provisional data as a preliminary assessment of their relative calibrations. As an additional check on their long-term stability, the VIRS data are compared to the broadband longwave radiances of the Clouds and the Earth's Radiant Energy System (CERES) scanners on *TRMM*. No statistically significant trend in the calibration of any of the three (3.7, 10.8, and 12.0 μm) VIRS thermal channels could be detected from the comparisons with CERES data taken during 1998 and 2000 indicating that the VIRS channels can serve as a reliable reference for intercalibrating satellite imagers. However, a small day–night difference in the VIRS thermal channels detected at very low temperatures should be taken into account. In general, most of the channels agreed to within less than $\pm$0.7 K over a temperature range between 200 and 300 K. Some of the smaller differences can be explained by spectral differences in the channel response functions. A few larger differences were found at 200 K for some of the channels suggesting some basic calibration differences for lower temperatures. A nearly 3-K bias in the ATSR-2 11-μm channel relative to VIRS and *GOES-8* was found at the cold end of the temperature range. The intercalibrations described here are being continued on a routine basis.

1. Introduction

Satellite infrared imagers are essential for measuring a variety of surface and atmospheric properties including cloud and sea surface temperatures. The accuracy of those quantities is directly dependent on the calibration of each infrared channel. Most spectral imagers on operational meteorological satellites use onboard blackbody references to monitor and adjust the calibration coefficients for thermal infrared channels on a relatively frequent basis. Differences in the calibration sources and methods and in the spectral filter functions from one satellite to the next can introduce differences in the temperatures that would be observed by a given pair of satellites for the same scene. Thus, cross calibration of the different infrared imagers and normalization to an absolute standard are necessary steps to ensure that

Corresponding author address: Patrick Minnis, NASA Langley Research Center, MS 420, Hampton, VA 23681.
E-mail: p.minnis@larc.nasa.gov

trends in a given quantity detected in data from multiple satellites are due to changes in the system and not the calibration. This type of approach was employed by Brest et al. (1997) who use the *NOAA-9* Advanced Very High Resolution Radiometer (AVHRR) channels 1 and 4 (11 μm) as the standards for the corresponding visible and infrared channels, respectively, on the series of satellite data used by the International Satellite Cloud Climatology Project. With the increase in the number of operational satellite imagers with multispectral infrared channels, it is necessary to normalize similar channels on different satellites so that they may also be used confidently in climate studies. In Part I of this paper (Minnis et al. 2002), the visible channels from a variety of satellites were normalized to the 0.65-μm channel on the Visible Infrared Scanner (VIRS; Barnes et al. 2000) on the *Tropical Rainfall Measuring Mission* (*TRMM*) satellite. Following a similar procedure, this paper examines the responses of three different infrared channels on VIRS relative to their counterparts on a selected set of satellites to gain a better understanding of the differences and to provide a reference and basis for applying the calibrations to other satellites, both past and future (Nguyen et al. 2001, submitted to *J. Atmos. Oceanic Technol.*, hereafter NG01).

Strong correlations exist between broadband longwave (LW) data and 11-μm radiances (e.g., Minnis and Harrison 1984; Minnis and Smith 1998; Doelling et al. 2001). Because of these correlations, any trends in the LW data should be mirrored in corresponding narrowband channels depending on the temporal variations in the spectral characteristics of the viewed scenes. Highly accurate broadband data should therefore be useful for monitoring trends in narrowband data. Broadband LW and window (WN) radiances were measured by the Clouds and Earth's Radiant Energy System (CERES; Wielicki et al. 1998) instruments on *TRMM* (Lee et al. 1998). The LW and WN radiances were calibrated with an onboard active blackbody and with space views. Continuous CERES data were taken by *TRMM* during the first 8 months and only sporadically between September 1998 and April 2000. Priestley et al. (2000) examined the stability of the CERES calibrations on the *TRMM* at various times between 1998 and 2000. Lyu et al. (2000) used deep space views to check the angular response of the VIRS thermal channels during 1998. Both studies found no significant trends in the calibrations.

Following Minnis et al. (2002), this paper correlates the VIRS solar-infrared (SIR; 3.777 μm), infrared (IR; 10.75 μm), and split window (SWC; 11.945 μm) radiances with the LW and WN channels of CERES to examine the relative stability of their long-term calibrations over a period of 2–3 yr, beginning in January 1998. The three VIRS infrared channels are then correlated with the corresponding narrowband channels on the second European Remote Sensing Satellite (*ERS-2*) Along Track Scanning Radiometer (ATSR-2; Mutlow et al. 1999) and the *Terra* satellite's Moderate Resolution Imaging Spectroradiometer (MODIS; Butler and Barnes 1998) for selected periods and with two of the thermal infrared channels on the fifth *Geostationary Meteorological Satellite* (*GMS-5*) for 1 yr. Additionally, the VIRS and ATSR-2 data are correlated with the relevant channels on the eighth *Geostationary Operational Environmental Satellite* (*GOES-8*). The results of this study should be valuable for understanding the long-term stability of these important sensors, to further evaluate the relationship between narrowband and broadband radiances, and to understand and correct for the differences in their measurements of infrared temperatures.

2. Data

The *TRMM* satellite operates at 350 km above the earth's surface in a precessing orbit with an inclination of 35°. Its sensors can observe at all local hours over a given location between roughly 37°N and 37°S during a 46-day period. *TRMM* was launched in November 1997 and all of the instruments became operational by 1 January 1998. The Earth Observing System *Terra* satellite was launched during December 1999 into a sun-synchronous orbit with a nominal equatorial crossing time of 1030 LT. *GOES-8* was launched 13 April 1994 and has been located at 75°W since September 1994. *GMS-5* was placed in operational service over the equator at 140°E during June 1995. The *ERS-2* was launched 21 July 1995 into a sun-synchronous orbit with a nominal equatorial crossing time of 1030 LT.

a. CERES

The CERES instrument has a nominal subsatellite resolution of 10 km from the *TRMM* altitude of 350 km and scans to a nadir angle of 90°. The scanner operates in both cross-track and rotating-azimuth plane modes. Only data taken in the former mode are used here. Lee et al. (1998) found that the calibrations of all three channels changed by less than $\pm 0.3\%$ from prelaunch to the initial on-orbit operations. Thomas et al. (2000) reported a 0% drift during the first 8 months of operation. The scanner was turned off during September 1998 and restarted for selective overpasses during 1999 and for the entire month of March 2000. Only the unfiltered radiances from 1998 and 2000 are used here. The uncertainties in the unfiltered LW (5–200 μm) and WN (8–12 μm) radiances are 0.2% and 1.0%, respectively. Each CERES radiance is tagged with one of three surface types for this study. These include ocean, land, and desert specified at a 2.5° resolution (Barkstrom et al. 1990).

b. VIRS

The VIRS (Barnes et al. 2000) scans up to a viewing zenith angle (VZA) of $\theta = 48°$ with a nominal subsatellite resolution of 2 km. The prelaunch and in-orbit

calibration procedures and results for the first year of operation were reported by Barnes et al. (2000) and Lyu et al. (2000), respectively. Version-5 VIRS radiances are used here. For comparison with CERES, the VIRS data were convolved into collocated CERES footprints using the CERES point spread function (Green and Wielicki 1995) to obtain a mean VIRS radiance L_{CV} for each CERES cross-track pixel out to $\theta = 48°$. The subscripts CV and x refer to VIRS–CERES and the VIRS channel number, respectively.

To compare with the other satellite data, the mean radiances L were computed for each box in a grid over the area of interest and converted to equivalent blackbody temperatures T using the Planck function. All of the data are averaged on a 0.5° grid for *GOES-8* and *GMS-5* and on a 0.25° grid for ATSR-2 and MODIS.

The nominal VIRS central wavelengths, λ_N, were determined by integrating the spectral response function $F(\lambda)$ over the wavelength λ for each channel:

$$\lambda_N = \frac{\int_{\lambda_1}^{\lambda_2} \lambda F(\lambda)\, d\lambda}{\int_{\lambda_1}^{\lambda_2} F(\lambda)\, d\lambda}, \tag{1}$$

where λ_1 and λ_2 are the respective minimum and maximum wavelengths where $F \geq 0.01$ and define the spectral bandwidth $\Delta\lambda$. The radiance is assumed to correspond to the Planck function $B_\lambda(T)$ evaluated at the nominal central wavelengths,

$$L_{\Delta\lambda} = B_{\lambda_N}(T). \tag{2}$$

Conversely, the temperature is determined by taking the inverse of the Planck function. For VIRS, the SIR, IR, and SWC nominal central wavelengths are 3.777, 10.751, and 11.944 μm, respectively.

Use of the Planck function with λ_N generally provides an accurate means for converting L to T. However, for wide bandwidths or for those where the Planck function varies rapidly with temperature, the use of the nominal central wavelength in the Planck function can cause some errors in the equivalent blackbody temperature compared to the original calibration. A more accurate central wavelength should take into account the variation of the Planck function with temperature. Thus, the radiance-weighted central wavelength for a given filter function varies with temperature,

$$\lambda_W(T) = \frac{\int_{\lambda_1}^{\lambda_2} \lambda B_\lambda(T) F(\lambda)\, d\lambda}{\int_{\lambda_1}^{\lambda_2} B_\lambda(T) F(\lambda)\, d\lambda}. \tag{3}$$

The spectral radiance at each temperature is

$$L_{\Delta\lambda}(T) = \frac{\int_{\lambda_1}^{\lambda_2} B_\lambda(T) F(\lambda)\, d\lambda}{\int_{\lambda_1}^{\lambda_2} F(\lambda)\, d\lambda}. \tag{4}$$

For the VIRS IR and SWC channels, the difference in T between (2) and (4) for the considered temperature range (180–330 K) is equal to or less than ±0.1 K. The difference is greater for the SIR channels where the Planck function varies substantially with L for the considered temperatures. To quantify the impact of using (2) instead of (4) for the SIR channels it is necessary to easily convert T to L and vice versa. Lyu et al. (2000) used linear interpolation on a lookup table based on (4) to obtain the relationship between radiance and temperature for the VIRS wavebands. The relationship can also be approximated by using (2) with an optimal central wavelength from (3) where the radiance is nearly the same for both (2) and (4) and then applying a temperature-dependent correction. The optimal central wavelength for the VIRS SIR channel is 3.788 μm. The temperature corresponding to a given VIRS SIR radiance is

$$T(L_{\Delta\lambda}) = 1.0041 B^{-1}_{3.787}(L_{\Delta\lambda}) - 1.132. \tag{5}$$

The difference between the VIRS SIR temperatures computed using (2) and (5) ranges from 0.7 K at 200 K to 0.3 K at 330 K.

Use of (5) is expected to be accurate for nocturnal observations. During the day, however, the solar spectral radiance, which is distributed with wavelength according to the Planck function at about 6000 K, introduces a different weighting than used in (4). The impact of solar reflectance on the spectral radiance distribution will vary with scene and solar zenith angle. Consideration of its effects on (4) is beyond the scope of this paper. For simplicity, unless otherwise noted, (2) is used here to convert VIRS radiances to temperatures and vice versa for all of the VIRS channels using the nominal central wavelengths. The impact of using (2) instead of (4) is discussed later.

c. GOES-8

The *GOES-8* 5-channel imager has 4-km SIR (3.911 μm), IR (10.703 μm), and SWC (11.947 μm) channels (Menzel and Purdom 1994) with data taken every 15 min at 10-bit resolution. The operational calibration procedures for *GOES-8* are described by Weinreb et al. (1997). The IR calibrations for radiance are quadratic in count as noted by Menzel and Purdom (1994). Radiance and temperature are related using (2). For matching with other satellites, the data are averaged on a 0.5° grid. The correlations with VIRS used only those collocated data that were matched to within ±15 min. Oceanic areas with significant sunglint were eliminated us-

ing the procedure outlined by Minnis et al. (2002) to minimize the impact of sunglint on daytime comparisons of SIR data. During the daytime, only those data with values of θ and relative azimuth angles that differed by less than 15° were used in the comparisons. No angular restrictions were imposed on matched nighttime IR data except that the values of θ could differ by no more than 5°. Except for some deep convective systems, all of the data were taken over ocean.

d. GMS-5

The *GMS-5* Visible Infrared Spin Scan Radiometer has 4 channels with a nominal resolution of 5 km. The *GMS-5* IR channel (10.806 μm, channel 2) covers the same spectral range as *GOES-8* with different weighting. The *GMS-5* SWC channel (11.499 μm, channel 3) is centered closer to 11.5 μm and spans the range from 10.7 to 12.4 μm. Temperature is converted to radiance with (2). Matching of the *GMS-5* and VIRS data follows the same procedures as those for *GOES-8.*

e. MODIS

MODIS, a 36-channel imager, began producing the first usable imagery on 18 March 2000. It scans to $\theta \sim 70°$ providing a swath width of 2330 km. This study uses only 1-km resolution MODIS MOD021KM provisional data (available online at http://modarch.gsfc.nasa.gov/MODIS/MODIS.html) taken with the ''B-side'' electronic configuration during November 2000 and January and March 2001. The provisional MODIS data, created during 2001, were calibrated in the same fashion between 1 November 2000 and 15 June 2001. The prelaunch calibration characteristics of the MODIS channels are discussed by Barnes et al. (1998). As of this writing, examination and validation of the MODIS dataset is continuing. Temperatures for the MODIS channels 20 (λ_N = 3.788 μm, λ_W = 3.792μm), 31 (λ_N = 11.014 μm), and 32 (λ_N = 12.03 μm) are correlated with their VIRS counterparts. VIRS and MODIS data are matched in the same fashion as the *GOES-8*–VIRS data with additional separate day and night datasets for the SIR channels. MODIS IR and SWC radiances are converted to temperature using (2). The temperature differences between (2) and (4) for the MODIS IR and SWC channels are less than 0.04 K. The SIR temperatures are estimated using

$$T(L_{\Delta\lambda}) = 1.0014B^{-1}_{3792}(L_{\Delta\lambda}) - 0.361. \quad (6)$$

The temperature difference between using (2) with λ_N and using (6) varies from 0.26 K at 180 K to 0.10 K at 330 K.

f. ATSR-2

The ATSR-2, a 7-channel radiometer on the *ERS-2*, produces a 555 × 512 image with a nominal resolution of 1 km. The ATSR-2 is a tilted conical scanner that creates a series of images that provide views of a given area twice during an overpass: once near nadir and once at $\theta = 55°$. Only the near-nadir view is used here. ATSR-2 data were selected if the subsatellite point was in the swath of the VIRS or *GOES-8* taken within 10 min of the *ERS-2* overpass. Only collocated data that matched to within $\pm 10°$ of θ were used in the correlations. Most of the ATSR-2 data used for the VIRS comparisons were taken over ocean surfaces during two periods: February–August 1998 and February–July 2000. Some data were taken over the Amazon Basin during the 1998 period to measure some optically thick clouds that increased the dynamic range. ATSR-2 data from selected months during 1995–99 were used in the *GOES-8* comparisons. The ATSR-2 data are provided as temperatures and are converted to SIR, IR, and SWC radiances using the respective nominal wavelengths, 3.7, 10.8, and 12.0 μm, in (2).

g. Spectral summary

A comparison of the SIR channels in Fig. 1a shows the large difference between *GOES-8* and the other three satellites. The MODIS band is centered within the VIRS band suggesting the two should be well correlated. Unlike the others, the ATSR-2 SIR includes wavelengths shorter than 3.6 μm. The IR bands are shown in Fig. 1b. MODIS, *GMS-5*, and ATSR-2 peak near 11.0 μm, while VIRS and *GOES-8* have a maximum at shorter wavelengths. *GOES-8*, *GMS-5*, and VIRS include significant amounts of energy between 10.1 and 10.5 μm, unlike either MODIS or ATSR-2. MODIS has the narrowest SWC filter, which peaks at 11.9 μm (Fig. 1c). ATSR-2, *GOES-8*, and VIRS have fairly similar SWC filters that overlap only about half of the *GMS-5* SWC channel. The latter includes no data beyond 12.3 μm.

3. Methodology

a. CERES–VIRS

A linear fit between the VIRS and CERES radiances is computed for each hour of data. Only data taken at night are used for the SIR–LW correlations. Both daytime and nighttime linear fits are computed for IR and SWC data. It is assumed that over the course of a year, the same sets of angles and scenes over a given surface type will have been sampled sufficiently to eliminate any scene or angular dependence in the fits. Additionally, fits for each dataset from March 1998 and March 2000 are compared because they should, in effect, measure similar sets of angles and conditions.

The CERES radiances L_C are regressed against the corresponding VIRS spectral radiances derived using the effective blackbody temperatures in the Planck function at the central wavelength to obtain a linear equation,

$$L_C = aL_{Vx} + b. \quad (7)$$

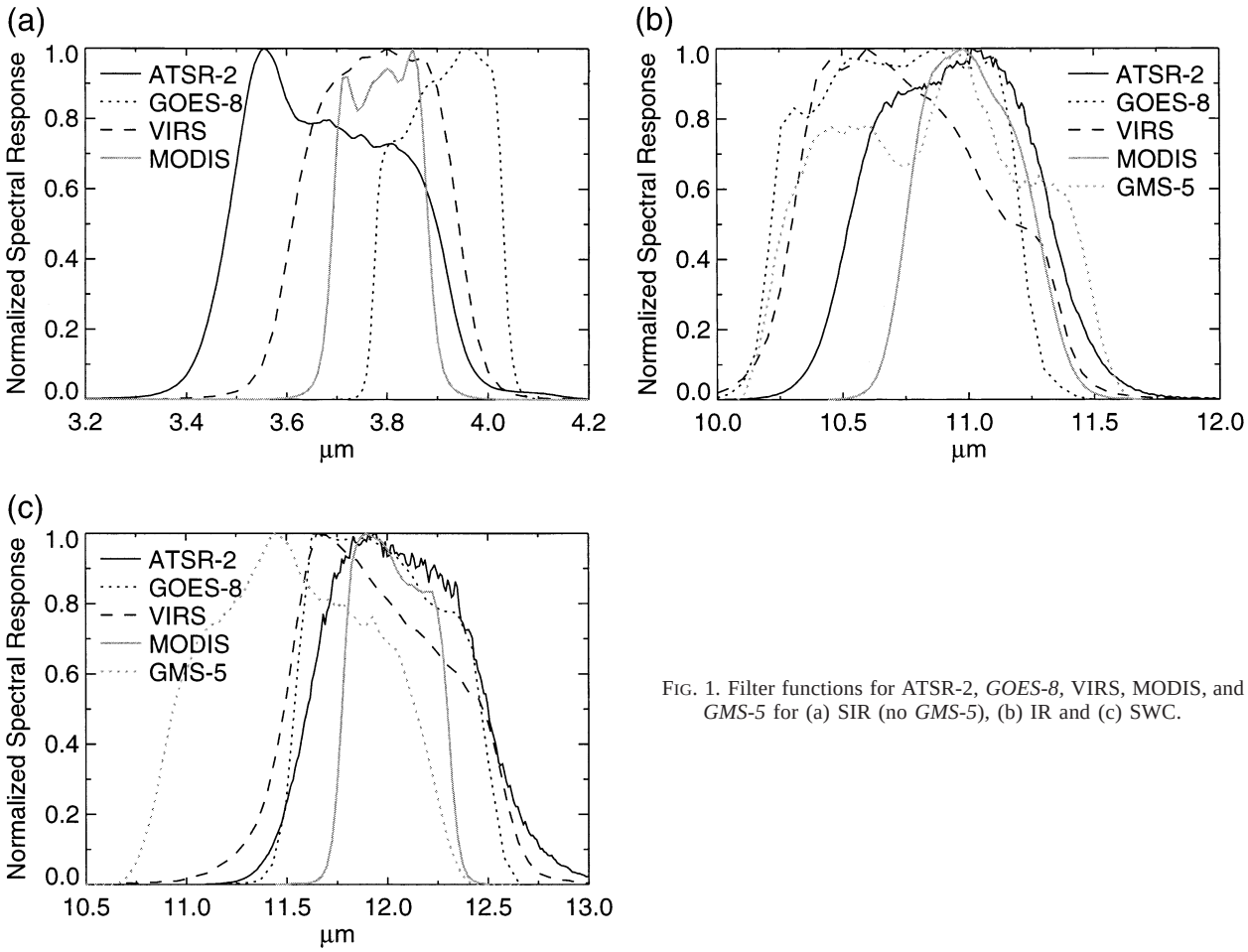

FIG. 1. Filter functions for ATSR-2, *GOES-8*, VIRS, MODIS, and *GMS-5* for (a) SIR (no *GMS-5*), (b) IR and (c) SWC.

The value of the slope a is in units of μm because the spectral radiance is used to approximate the narrowband radiance as in (2). Trends in a and the offsets b are then computed for the entire time period along with statistical parameters to determine the significance of the resulting trends.

b. GOES-8–*VIRS–ATSR-2*

The SIR, IR, and SWC mean equivalent blackbody temperatures T from the paired satellites are regressed using a least squares technique to obtain a linear equation for each satellite pair and channel:

$$T_{Vi} = cT_{Gj} + d, \quad (8)$$

$$T_{Ai} = cT_{Gj} + d, \quad (9)$$

$$T_{Vi} = cT_{Aj} + d, \quad (10)$$

where c and d are the slope and offset, respectively. The fits are performed for each pair of appropriate channel numbers i and j. Trend lines of slope and offset were computed for the VIRS–*GOES-8* results.

*c. VIRS–MODIS, VIRS–*GMS-5

The VIRS and MODIS thermal datasets are correlated as in (8) using the MODIS equivalent blackbody temperatures, T_{Mj}. VIRS and *GMS-5* IR and SWC data are correlated as in (8) using T_{GMj}. No trend lines are computed for the MODIS results because of the short period of available data.

4. CERES–VIRS results and discussion

Despite the lack of solar radiation in the nocturnal 3.7-μm data, the LW radiance varies by as much as a factor of 2 for a given value of L_{V8} (Fig. 2a). Conversely, for a given value of LW radiance, L_{V2} can vary by up to a factor of 4. The LW radiance is primarily determined by cloud height, optical depth and atmospheric humidity while the SIR radiance is also quite sensitive to cloud phase and particle size. The relationship between the SIR and LW channels is not linear because the Planck function rapidly approaches zero at 3.7 μm for the very low cloud temperatures while the LW radiance remains significant because of contributions from

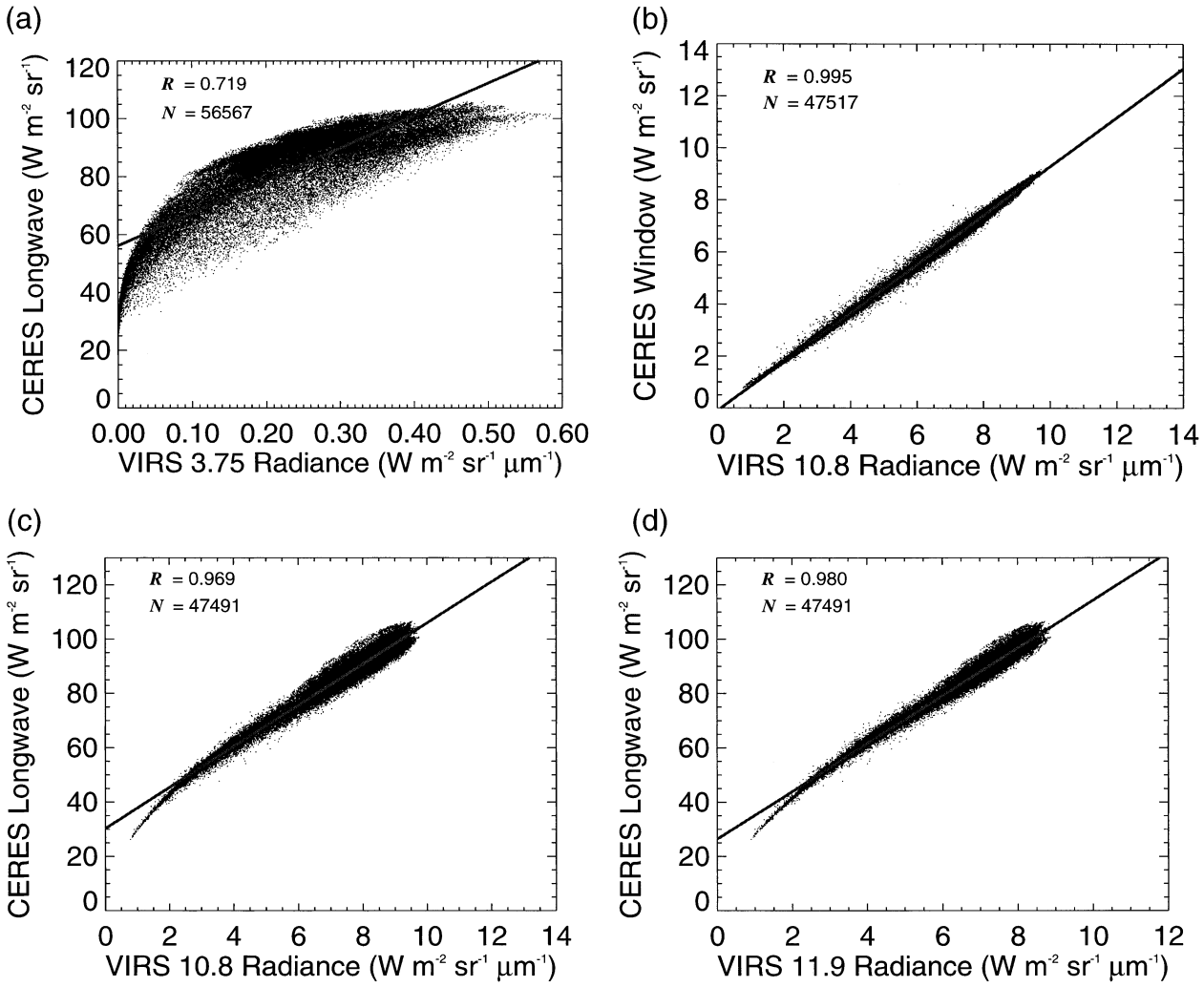

FIG. 2. Correlation of radiances at night. (a) CERES LW and VIRS SIR, (b) CERES LW and VIRS IR over ocean, (c) CERES LW and VIRS SWC over ocean and (d) CERES WN and VIRS IR over ocean.

longer wavelengths. Although the relationship is more linear for the IR and SWC channels (Figs. 2b,c), the rate of change of LW radiance with the spectral radiances is much greater at the lowest temperatures than it is for higher temperatures. This difference at the cold (low radiance) end of the graph has been recognized and requires a nonlinear fit to estimate LW from IR data (e.g., Minnis et al. 1991). Linear fits are used here to facilitate detection of trends. The variation of LW for a given value of L_{V5} is smaller than for a given value of L_{V4} because the SWC channel is more sensitive to water vapor absorption, a parameter that significantly affects the LW radiance. The SWC correlation coefficient is slightly greater than its IR counterpart suggesting that it may be more appropriate than the IR data for estimating the LW flux. Figure 2d shows that the IR and WN data are better correlated presumably because of their smaller spectral differences.

Time series and the corresponding trend lines were computed for all of the daily matched data for each channel and surface type. The marine daytime LW–IR gain variations in Fig. 3 hint at a slight degradation in the IR calibration. Table 1 summarizes the apparent degradation rates over ocean for all of the channels giving values for the average gain a_m, the mean offset b_m, the computed rate of change in gain Δa, the initial fitted gain a_o at 1 January 1998, and the squared linear correlation coefficient R. The SIR gain appears to have decreased at a rate of roughly 10% yr^{-1} and 5% yr^{-1} over ocean and land, respectively, perhaps due to seasonal variation in the scenes viewed by the sensor. The mean IR–LW slopes are almost identical for both day and night and both gains show an apparent decrease of $\sim$1% yr^{-1}. A comparable increase is seen over land, however, suggesting a slight seasonal dependence. Using the WN channel in the IR regressions results in a mean slope change of less than -1% yr^{-1}. The SWC channel comparisons to the LW data yield a mean de-

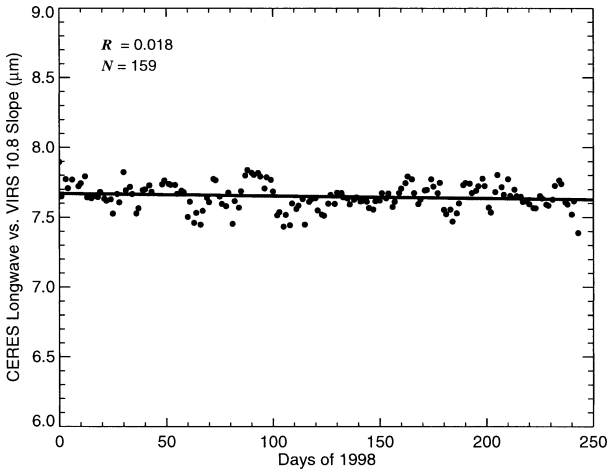

FIG. 3. Time series of daily mean slope in linear fits between CERES LW and VIRS IR radiances.

crease of less than 0.5% yr^{-1} over ocean and slightly larger increases over land.

Because the 8-month datasets do not provide a complete annual cycle, variations in surface and cloud conditions may not be completely sampled and could produce trends like those in Fig. 3. If seasonal sampling effects are the sole cause of the trends seen in Table 1, then the mean slopes taken during the same month in two different years should be equivalent because similar times of day are sampled over a given region during the month. Table 2 lists the slopes and offsets for each of the channels over ocean for March 1998 and 2000. Using the fits for these 2 months over the full range of observed narrowband values, the LW radiances computed from the SIR fits increased by 0.1% over ocean. The 0.1% yr^{-1} decrease in the SIR-channel gain is considerably less than the 10% change found in Table 1 indicating that seasonal variations were driving the large apparent degradation rate. The mean LW radiance computed with the IR channel decreased by 0.3% and increased by 1.4% during day and night, respectively. Corresponding changes from the SWC fits yield 0.2% and −0.1% changes, respectively. The WN radiances decrease by an average of 0.3% for a given IR radiance during the 2-yr interim. All of these differences are within the uncertainties of the fits for the two months of data and, therefore, no statistically significant trends are detected with this approach for any of the VIRS channels.

Despite some apparent trends in the 8-month datasets, the CERES–VIRS March 1998 and 2000 correlations for each of the VIRS channels suggest that the VIRS calibrations are stable and that the VIRS calibration procedures account for any significant degradation in the sensor components. A complete annual cycle of matched data would be more desirable for comparison but it is not available. Narrowband–broadband correlations also do not necessarily constitute an ideal means for assessing the calibration. Their utility depends on how well the quantities are correlated. Certainly, over ocean the surface spectral variations are minimized so that atmospheric conditions are the main source of variability. Figure 2 demonstrates that the broadband radiances are better suited for assessing the IR and SWC channels than for monitoring the SIR calibrations. However, if it is assumed that the conditions sampled over ocean are statistically the same between one time period and another, then highly correlated parameters like all of those examined here should yield the same relationship. One means for assessing the differences in Table 2 is to determine if they are beyond the expected variations in the monthly mean slopes. The standard deviations of the differences between the 8-month mean slopes and the monthly mean slopes are 3.5%, 0.5%, and 0.4% for the SIR, IR, and SWC fits, respectively. All of the differences over ocean surfaces in Table 2 are within one standard deviation of the month-to-month variability. Using a different approach, Lyu et al. (2000) found that all of the VIRS channel calibrations were stable during the first 11 months of operation. Based on these CERES comparisons, it is concluded that the onboard systems properly adjusted the VIRS calibrations to account for any sensor degradation throughout the first 27 months of operation. Thus, there has been no significant change in the VIRS performance during that period.

5. Results and discussion

In this section, the discussion of the results and the various errors in the calibrations is presented in terms of equivalent brightness temperatures. All of the sensors measure radiance, a quantity that is nonlinearly related to brightness temperature. Thus, the brightness temperature errors resulting from a given radiometric error will

TABLE 1. Trends in gain for linear fits between VIRS and CERES radiances over ocean, Jan–Aug 1998.

VIRS–CERES	Condition	a_o (μm)	Δa (μm day^{-1})	a_m (μm)	b_m	R
SIR–LW	Night	101.4	-2.97×10^{-2}	97.75	58.7	0.143
IR–LW	Day	7.67	-1.81×10^{-4}	7.649	29.6	0.018
	Night	7.66	-2.06×10^{-4}	7.630	30.3	0.016
IR–WN	Day	0.940	-0.29×10^{-4}	0.937	−0.108	0.102
	Night	0.937	-0.18×10^{-4}	0.935	−0.087	0.114
SWC–LW	Day	8.869	-1.69×10^{-4}	8.848	26.1	0.016
	Night	8.891	-1.30×10^{-4}	8.875	26.2	0.008

TABLE 2. Comparison of CERES broadband radiances to VIRS narrowband radiance regression between Mar 1998 and Mar 2000 for cross-track CERES footprints over ocean using a minimum of 340 000 observations.

Category time	Slope (μm)			Intercept		R	
	1998	2000	% diff	1998	2000	1998	2000
				LW vs 3.75 μm			
Night	99.62	99.41	−0.21	57.82	57.79	0.876	0.865
				LW vs 10.8 μm			
Day	7.623	7.669	0.60	29.95	29.54	0.980	0.977
Night	7.641	7.610	−0.41	30.13	31.13	0.980	0.978
				LW vs 11.9 μm			
Day	8.840	8.855	0.11	26.27	26.14	0.987	0.985
Night	8.886	8.817	−0.78	26.06	26.34	0.987	0.985
				WN vs 10.8 μm			
Day	0.937	0.939	0.28	−0.844	−0.104	0.997	0.997
Night	0.936	0.937	0.14	−0.079	−0.093	0.997	0.997

be different at high temperatures than at low temperatures. The following analyses attempt to account for the nonlinear effect when appropriate.

a. Solar-infrared channels

Figure 4 shows examples of the correlations between the *GOES-8* and VIRS SIR channels for February 2001. Daytime SIR temperatures are generally greater than those observed at night because of the added solar reflectance during the day. The daytime VIRS SIR temperatures in Fig. 4a are generally less, by 2.2 K on average, than those from *GOES-8*. The slope and offset of the regression line are 0.930 and 22.9 K, respectively, with $R = 0.917$ and an rms difference of 1.0%. At night (Fig. 4b), $R = 0.985$ and the mean difference is only −0.4 K. For this case, the slope and offset are 0.999 and 0.64 K, respectively. Some temperature differences between the *GOES-8* and VIRS channels are expected because spectrally dependent absorption lines and a mixture of two different source functions (solar reflected and surface–cloud–atmosphere emitted) on opposing tails of the Planck function produce significant differences in the brightness temperatures during the daytime. At night, only the emitted components are involved and the small difference may arise from differences in the absorption lines included within the respective spectral bands (Fig. 1a). Trend lines were computed for the time series of the coefficients and mean differences. Small, but compensating trends were found in the slope and offset such that the mean differences changed by less than 0.2 K over a 1200-day period. It was concluded that there is no significant trend in the *GOES-8* channel-2 calibration. The average coefficients for both the

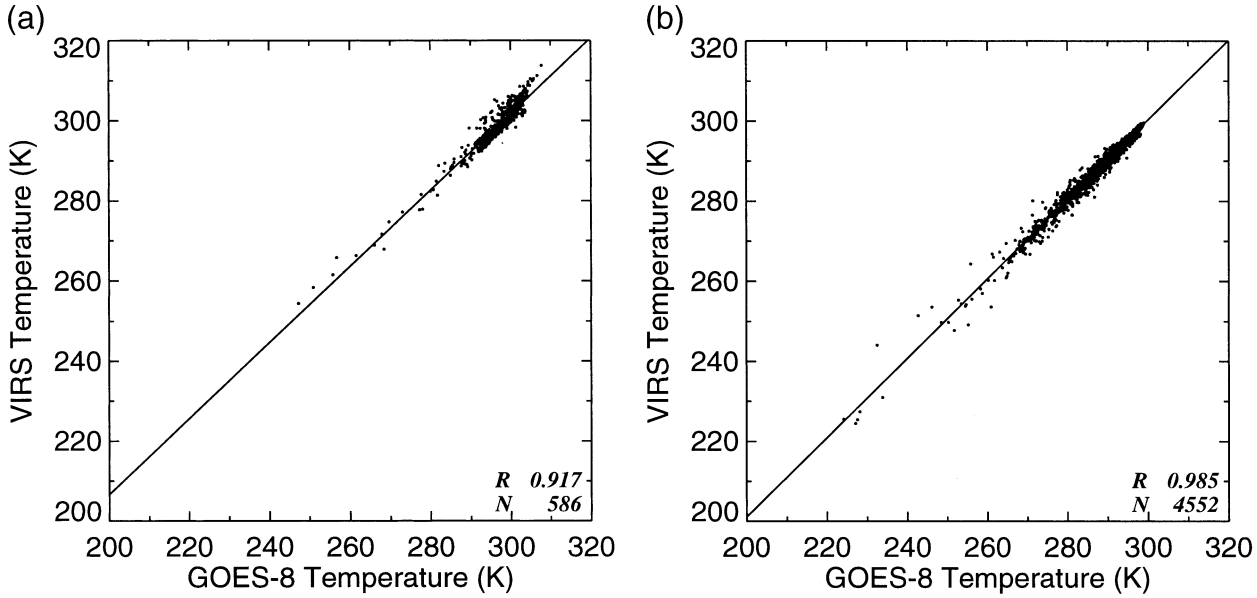

FIG. 4. Correlation of VIRS and *GOES-8* SIR data, Feb 2001. (a) Daytime and (b) nighttime.

TABLE 3. Mean regression coefficients and difference for VIRS and other satellite SIR temperatures.

Satellite channel	c	d (K)	ΔT	Std dev in c (%)
VIRS–*GOES-8* (day)	0.890	34.8	−2.77 K	4.1
VIRS–*GOES-8* (night)	1.0048	−0.75	−0.59 K	1.8
VIRS–MODIS (day)	1.0248	−8.00	−0.69 K	n/a
VIRS–MODIS (night)	1.0154	−4.42	−0.04 K	n/a

nighttime and daytime fits for the 4-yr period are listed in Table 3.

The number of ATSR-2 SIR data points is not sufficient for regression with either the *GOES-8* or VIRS data because many of the ATSR-2 values were missing. However, differencing the SIR data available during July 1995 revealed that the *GOES-8* temperatures exceeded their ATSR-2 counterparts by an average of 2.4 K, a value within the range of differences found for the VIRS–*GOES-8* datasets.

Figure 5 shows that the daytime and nighttime MODIS SIR temperatures are very close to their VIRS counterparts for March 2001. VIRS data with $T_{V3} > 319.5$ K are not used because the maximum VIRS channel-3 temperature, ~320 K, is recorded even in saturation conditions. The MODIS SIR temperatures saturate around 335 K. The slope of 1.0188 and offset of −6.0 K for the 646 data points in Fig. 5a are typical for the daytime results. At night (Fig. 5b), the fit is very similar with a slope of 1.0208 and an offset of −6.0 K. The mean slopes, offsets, and differences are shown in Table 3. Although the mean differences are very small, especially at night, the MODIS temperatures are generally larger than the VIRS values for $T < 250$ K.

The small differences between the *GOES-8* and VIRS and the MODIS and VIRS SIR temperatures may be due to either spectral differences or to some absolute calibration errors in one or the other instrument. To estimate the expected spectral differences, assuming a uniform surface emissivity, SIR TOA brightness temperatures were calculated for the three sensors using the correlated *k*-distribution coefficients from the technique of Kratz (1995) for two VZAs (20° and 50°) and two standard atmospheres: midlatitude winter (MLW) and summer. The routines for using the correlated *k*-distribution coefficients for the relevant MODIS, *GMS-5*, *GOES-8*, ATSR-2, and VIRS are available online (see http://asd-www.larc.nasa.gov/~kratz/). A thermally black surface was assumed for the clear sky case. The cloud emittance parameterizations of Minnis et al. (1998) for AVHRR were used to simulate the radiances for a water droplet cloud at 285 and 265 K with an effective radius of 12 μm and an ice cloud at 235 and 210 K with an effective diameter of 24 μm. The AVHRR emittances are nearly identical to those for VIRS. The emittance parameterizations for *GOES-8* (Minnis et al. 1998) were also used to determine the impact of spectral differences in cloud properties on the brightness temperatures. The calculations using the *GOES-8* emittance parameterizations yielded temperature differences that are negligibly different from those in Table 3 for the *GOES-8* theoretical fits. The computations were per-

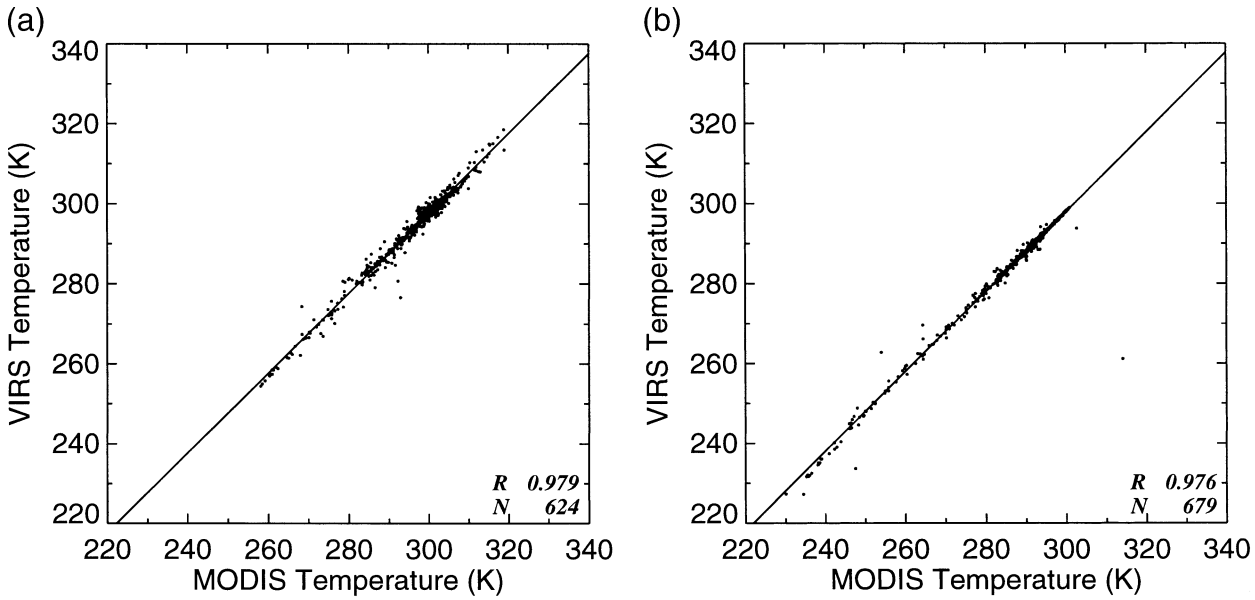

FIG. 5. Correlation of VIRS and MODIS SIR temperatures, Mar 2001. (a) Daytime and (b) nighttime.

TABLE 4. Theoretical linear regression coefficients and theoretical and observed brightness temperature differences between satellite SIR channels for nighttime conditions.

	Coefficients for $T_{V3} = cx + d$				
x	c	d (K)	T_{V3}	Theoretical $T - T_{V3}$ (K)	Observed $T - T_{V3}$ (K)
T_{G2}	0.9940	1.41	200	−0.2	−0.2
			300	0.4	−0.7
T_{M20}	0.9998	0.06	200	0.1	1.3
			300	0.1	−0.2

formed for a range of cloud optical depths at the appropriate altitudes within one or both atmospheric profiles (a cloud at 285 K could not be used in the MLW profile). The correlated k distributions were used to compute the absorption and emission within each layer above and below the cloud. The two atmospheric profiles with the four cloud cases should account for most of the conditions observed by the matched satellites.

Table 4 lists the coefficients resulting from the fits to the model data and the temperature differences at $T_{V2} = 300$ K and $T_{V3} = 200$ K along with the differences at those same temperatures computed from the average *GOES-8* and MODIS fits. The *GOES-8* cloud emittance models were used for the GOES data. The temperature differences, $T_{G2} - T_{V3}$, from the theoretical calculations indicate that VIRS should observe slightly warmer temperatures at the cold end of the scale and slightly colder ones at the hot end. The nighttime mean fit in Table 3 yields values of T_{G2} that agree with the theory at the cold end but are too low by 1.1 K at the warm end. If T_{V3} is computed using (5), presumably the more accurate calibration method, then the difference between VIRS and *GOES-8* reduces to 0.7 K at 300 K and the difference at 200 K increases to 0.7 K between the theoretical and observed temperature differences. The theoretical differences between MODIS and VIRS, T_{M20}, $-T_{V3}$, vary from −0.1 to 0.4 K, values that are slightly less than the observed nighttime differences. At the cold end of the scale, the mean fit yields T_{M20}, $-T_{V3} = 1.3$ K a value that exceeds the theoretical difference by 1.2 K. Using (5) for T_{V3} yields nearly perfect agreement between theory and observations at 300 K for the VIRS–MODIS comparison, but widens the gap at 200 K to a 2 K overestimate by MODIS relative to VIRS. The daytime differences for MODIS should be similar to those at night because the MODIS band is near the middle of the VIRS band unlike the *GOES-8* filter, which peaks outside of the VIRS SIR band.

The comparisons suggest that some of the observed differences between the *GOES-8* and VIRS SIR data can be explained by the spectral differences, but the high-temperature differences reveal a possible 1-K bias in one of the instruments. Because the bias is within the typical absolute accuracies of ±2 K at $T = 300$ K for the VIRS thermal channels (Lyu et al. 2000), it is not considered to be significant enough to warrant a correction. However, for consistency between the two instruments, it may be necessary to adjust the *GOES-8* calibration slightly if VIRS is considered as the reference. The low-temperature difference for the MODIS–VIRS data cannot be explained by the spectral differences suggesting a possible low-temperature bias. Again, this difference at 200 K is within the 2.6% uncertainty estimate of Lyu et al. (2000) for VIRS. Because the MODIS channels are in the final stages of postlaunch calibration, the cold-end difference may be eliminated in future MODIS datasets.

b. Infrared and split-window channels

The *GOES-8* and VIRS IR channel filter functions (Fig. 1b) are more similar spectrally than those for the corresponding SIR channels and, hence, should yield smaller temperature differences. The mean difference between the temperatures in Fig. 6a is only 0.5 K and the gain and offsets are 1.004 and −1.5 K, respectively. The temperature differences between the two instruments increase with decreasing temperature such that *GOES-8* temperatures are more than 1 K greater at 220 K but are in agreement around 315 K. The SWC channels for *GOES-8* and VIRS are also very similar (Fig. 1c) resulting in nearly the same temperatures for both channels (Fig. 6b). The mean difference of 0.7 K and the value of R, 0.994, in Fig. 6b are typical of all months for the *GOES-8* and VIRS channels 5. For this SWC case, the respective slope and offset are 1.008 and −2.9 K, respectively.

The IR slopes and offsets computed for each month vary over a range of 0.05 and 4 K, respectively, and are anticorrelated. As in the case for the SIR channels, an increase in gain is generally compensated by a decrease in the offset such that the mean differences between the *GOES-8* and VIRS IR temperatures are less than 0.5 K for each of the datasets. As shown in Table 5, the *GOES-8* IR temperatures exceed their VIRS counterparts by an average of 0.3 K for the entire period. The variations in the SWC slopes and offsets over the 38-month period are similar to those for channel 4. Overall, the mean difference between the VIRS and *GOES-8* SWC channels is −0.6 K. The mean slopes and offsets for both channels are listed in Table 5. Only regression fits with $R > 0.97$ were included in the averaging for Table 5 to preclude inclusion of those data that did not cover a substantial dynamic range or lacked a sufficient number of samples. Only one dataset was

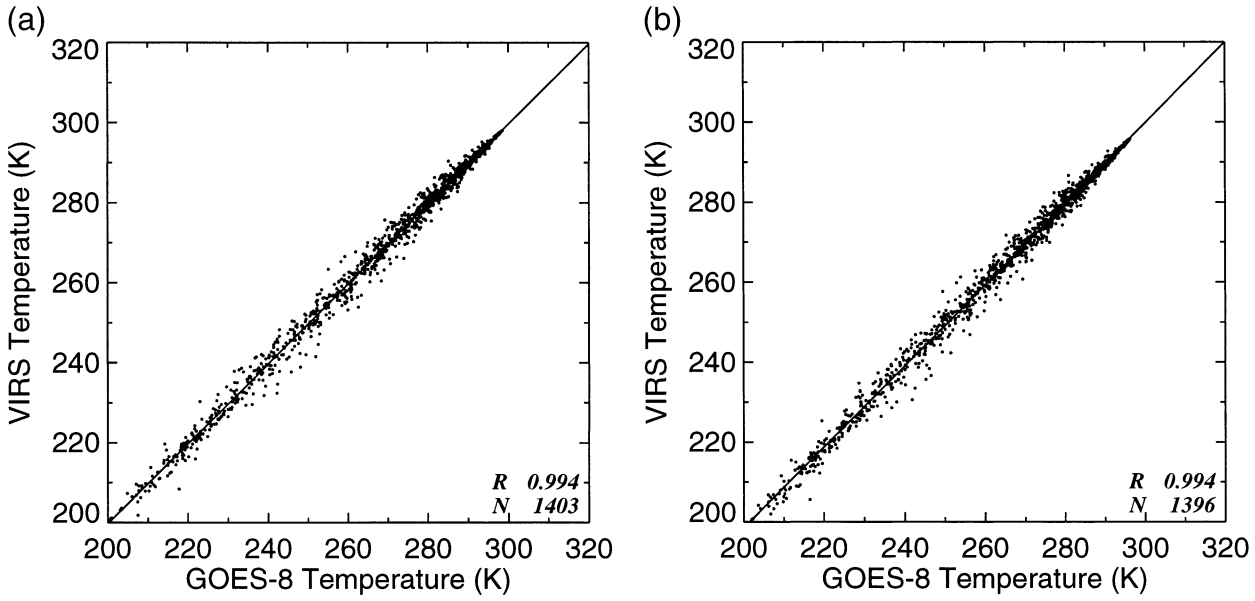

FIG. 6. Correlation of VIRS and *GOES-8* data, Feb 1998. (a) IR and (b) SWC.

eliminated in this fashion. No significant trends were found in the gains for either channel.

A fit to the matched VIRS and ATSR-2 IR channels for the 2000 dataset is shown in Fig. 7 with the data. The IR temperatures agree well at high temperatures but the VIRS measures higher temperatures than ATSR-2 as T decreases. A similar variation was seen in the SWC temperatures (not shown), although the differences are smaller at the cold end of the range. Table 5 lists the mean fits for the two matched VIRS–ATSR-2 thermal-channel datasets. All of the fits are based on highly correlated data with $R > 0.990$. Despite the relatively wide range in the values of c and d, the mean temperature differences are quite small, averaging -0.3 and 0.2 K for the IR and SWC bands, respectively. These mean differences do not necessarily reflect the true average behavior because most of the data have $T > 260$ K.

Figure 8 shows the data and regression fits between the *GOES-8* and ATSR-2 IR and SWC temperatures. The *GOES-8* temperatures closely match those of the ATSR-2 at high temperatures for both channels, but exceed them by 2 and 4 K for channels 4 and 5, respectively at 200 K. Table 5 lists the average slopes and offsets for the IR and SWC channels. No trends were detectable in the relationship between the *GOES-8* and ATSR-2 thermal channels. Using the average regression coefficients, T_A exceeds its *GOES-8* counterparts for $T_G = 300$ K by 0.1 and 0.0 K for the IR and SWC channels, respectively. On average, when $T_G = 200$ K, T_A is 196.2 K and 197.6 K for the same channels. These results, based on a wide range of temperatures, are consistent with the VIRS–ATSR-2 results.

Figure 9 shows the fits for the matched March 2001 daytime VIRS and MODIS IR and SWC data. The slope and offset for the IR channels (Fig. 9a) are 0.9930 and 2.20 K, respectively, and the mean difference is 0.1 K. These results are comparable to values in Table 5, which lists the mean slope, offset, and differences computed from all of the individual correlations for each of the matched datasets. The SWC data are also very close as

TABLE 5. Mean linear regression and difference statistics for the thermal infrared channels using combined day and night data.

Spectral band	Instruments (y/x), year	c	d (K)	ΔT ($T_y - T_x$) (K)
IR	VIRS–*GOES-8*, 98–01	1.0046	−1.60	−0.3
	VIRS–ATSR-2, 98	1.0176	−4.9	−0.1
	VIRS–ATSR-2, 00	0.9318	20.0	−0.5
	ATSR-2–*GOES-8*, 95–99	1.0391	−11.60	−0.6
	VIRS–MODIS, 0–01	0.9961	1.24	−0.2
	VIRS–*GMS-5*, 00–01	1.0195	−5.22	−0.1
SWC	VIRS–*GOES-8*, 98–01	1.0080	−2.77	−0.6
	VIRS–ATSR-2, 98	1.0267	−7.9	0.4
	VIRS–ATSR-2, 00	0.9569	12.0	0.0
	ATSR-2–*GOES-8*, 95–99	1.0244	−7.28	−0.5
	VIRS–MODIS, 00–01	1.0000	−0.745	−0.8
	VIRS–*GMS-5*, 00–01	1.0090	−4.07	−1.7

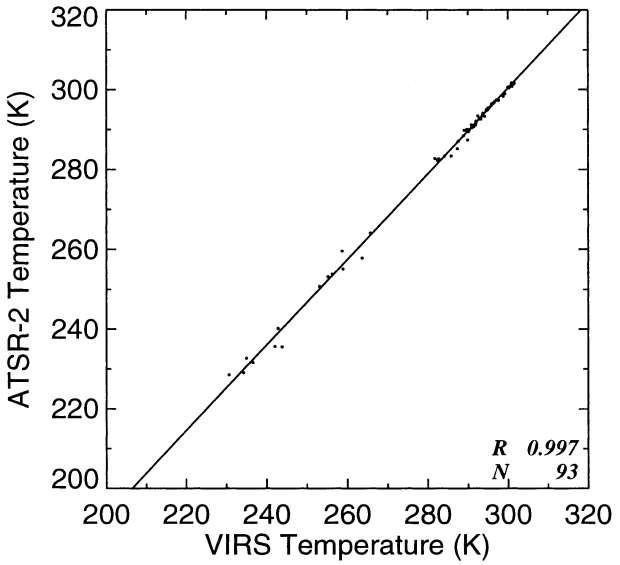

FIG. 7. Correlation of VIRS and ATSR-2 IR temperatures, Feb–Jul 2000.

indicated by $c = 0.9965$ and $d = 0.12$ K for the linear fit in Fig. 9b. In this case, T_{V5} averages 0.87 K less than T_{M32}. The 3-month daytime SWC mean values for c and d are 0.9960 and 0.33 K, respectively with an average difference between T_{V5} and T_{M32} is -0.79 K. The nighttime coefficients for the IR and SWC fits are $c = 1.0058$, $d = -1.59$ K and $c = 1.0038$, $d = -1.81$ K, respectively.

The comparisons between the VIRS and *GMS-5* IR and SWC data are similar to those for the other satellites. The value of R exceeds 0.980 for 81% of both IR and SWC regressions, which substitute T_{GM} for T_G in (2). The mean IR and SWC slopes and offsets for the 13-month period are given in Table 5. No bias is apparent in the IR data. On average, the *GMS-5* SWC temperatures are 1.65 K greater than those from VIRS.

To estimate the expected differences between the temperatures from VIRS and the other satellites, calculations were performed for theoretical cases following the approach used for the SIR channels using the AVHRR cloud emittance parameterizations for all cases. The results are summarized in Table 6, which shows fits between the theoretical VIRS and other imager temperatures and a comparison of the temperature differences computed from the theoretical and mean observed fits as in Table 4. The average fits for all of the data, both day and night, were used for a given satellite. Over the range from 200 to 300 K, the differences between VIRS and the *GOES-8* and MODIS IR temperatures are within ± 1.0 K of the values expected from the theoretical calculations. The *GMS-5* and ATSR-2 IR temperatures are also within 1 K of the theoretical values at 300 K. However, both instruments yield temperatures that exceed the theoretical values relative to VIRS by more than 1.4 K at $T_{V4} = 200$ K. The differences between the model and observed fits are less than ± 1 K for the MODIS and ATSR-2 SWC channels over the 100-K temperature range. The *GOES-8* and *GMS-5* SWC fits are close to the theoretical results for high temperatures but exceed the theoretical value by 1.2 and 2.5 K, respectively, at 200 K.

Temperature differences smaller than 1.0 K may simply be the result of the absolute accuracy of a given temperature measurement, which typically is given as ± 1.0 K (e.g., Menzel and Purdom 1994). Thus, all of the sensors agree to within the absolute accuracy of the

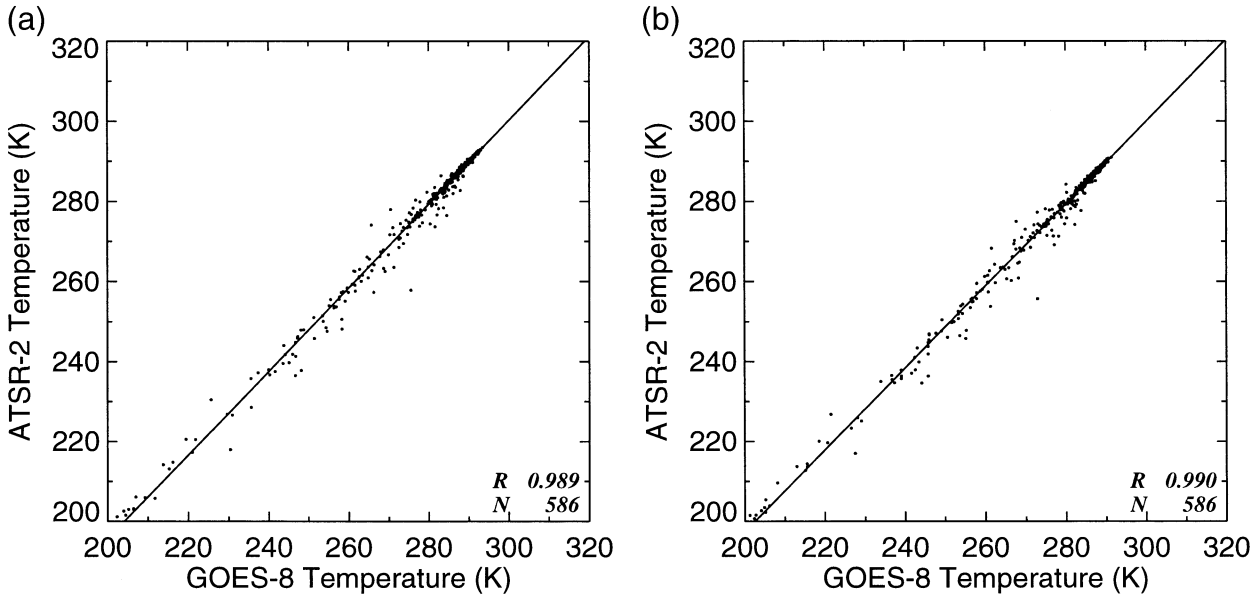

FIG. 8. Correlation of *GOES-8* and ATSR-2 channels, Jul 1995. (a) IR and (b) SWC.

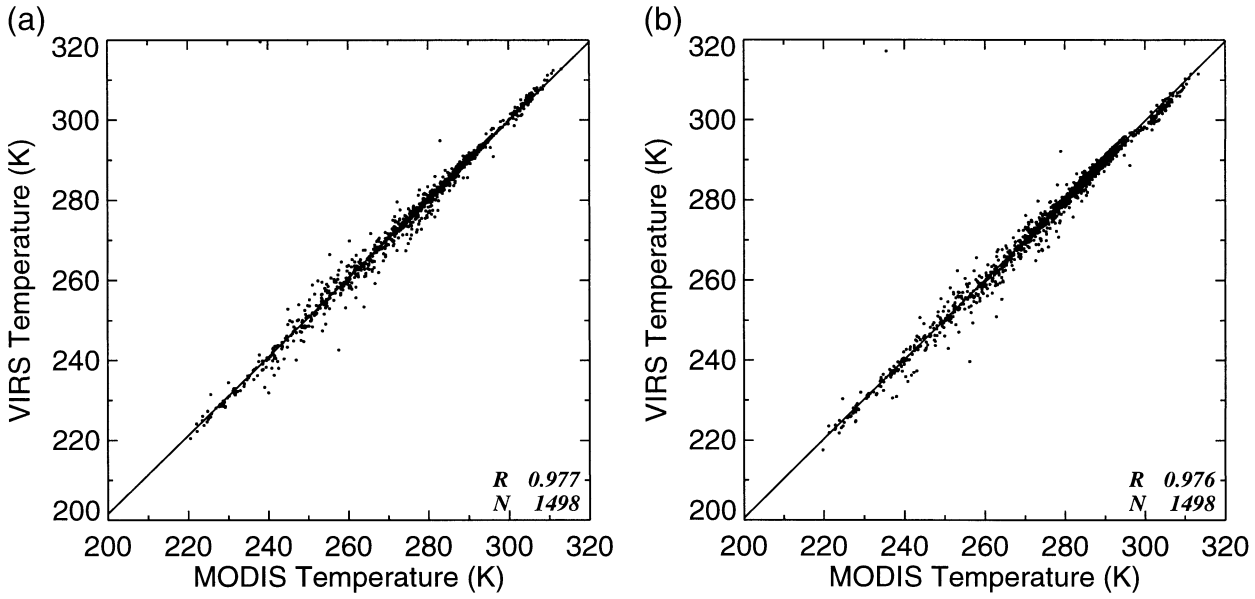

FIG. 9. Correlation of VIRS and MODIS daytime temperatures, Mar 2001. (a) IR and (b) SWC.

measurement systems at high temperatures, while some disagreement remains for some of the imagers at low temperatures. Noise in a given SIR or SWC measurement, which may vary from 0.25 K for MODIS (Barnes et al. 1998) to 0.4 K for *GOES-8* (Menzel and Purdom 1994), should not be a factor in these correlations because each data point represents an average over many pixels. Other factors that could affect these correlations are diurnal variations in the sensor heating due to some solar warming (e.g., Trischenko and Li 2001), and changes in the spectral radiance distribution due to cloud particle size variations.

In Fig. 6, which includes both day and night values, the *GOES-8* and VIRS IR and SWC temperatures differ by only 1.2 K or less at 200 K and agree well at higher temperatures. If only nighttime data are used, the average slope and offset are 1.0096 and −2.98 K, respectively, for the IR and 1.0105 and −3.37 K for the SWC. Given these mean fits, T_{V4} is 0.1 K less than T_{G4} and T_{V5} is 1.6 K less than T_{G5} at $T_G = 200$ K. At 300 K, T_{V4} and T_{V5} are 0.1 and 0.5 K less, on average, than their *GOES-8* counterparts. During the daytime, T_V and T_G are slightly closer. The values of $T_V - T_G$ from the separate day and night fits were compared for $T = 300$

TABLE 6. Theoretical linear regression coefficients and theoretical and observed brightness temperature differences between satellite IR and SWC channels

	Coefficients for $T_V = cx + d$			Theoretical	Observed
x	c	d (K)	T_{V3}	$T - T_{V3}$ (K)	$T - T_{V3}$ (K)
IR					
T_{G4}	0.9928	1.78	200	−0.3	−0.6
			300	0.4	−0.5
T_{MB1}	0.9952	1.04	200	−1.0	0.0
			300	−1.0	−0.4
T_{AT4}	0.9960	0.95	200	−0.2	2.7
			300	0.2	0.0
T_{GM2}	0.9955	0.98	200	−0.1	1.3
			300	0.4	−0.6
SWC					
T_{G5}	1.0016	−0.36	200	0.0	1.2
			300	−0.1	0.4
T_{M32}	0.9941	1.26	200	−0.1	0.7
			300	0.5	0.8
T_{AT5}	1.0039	−0.71	200	−0.1	0.5
			300	−0.5	−0.4
T_{GM3}	0.9877	2.78	200	−0.3	2.2
			300	0.9	1.4

K with the results of calculations for theoretical cases given in Table 6. The absolute differences at $T = 200$ K, however, are significantly greater than the theoretical calculations, ranging between -0.5 K for the daytime IR and -1.6 K for channel 5 during day and night. The discrepancy between the T_G and T_V at low temperatures might be due to particle size effects within cold clouds or possibly to diurnal changes in the sensors (see next section). Further study is needed to understand the low-temperature differences.

The large IR and SWC differences at $T = 200$ K for ATSR-2 and *GOES-8* are not likely to be the result of small ice crystals at the tops of the thick cold clouds. Smith et al. (1998) showed that, for thin cirrus clouds with small ice crystals, the brightness temperature at 10 μm is much greater than at 11 μm, but is only $\sim$1 K greater for thick ice clouds with large particles. The ATSR-2 IR filter function includes no radiation between 10.0 and 10.5 μm, while approximately 20% of the VIRS and 33% of the *GOES-8* IR radiation is from the 10.0–10.5-μm interval. The particle size effect is probably not sufficient to explain the nearly 4-K difference between T_G and T_A at 200 K because that temperature would only be observed for an optically thick cloud. Inclusion of the $\sim$0.5-K bias at 200 K from the daytime VIRS–*GOES-8* fits would only slightly reduce the difference in Fig. 8 to a value closer to that between *GOES-8* and ATSR-2. Given the consistency between VIRS and *GOES-8,* the large differences at the cold end of the temperature range for both the IR and SWC channels suggest that the ATSR-2 cold reference blackbody calibration source may be biased.

c. VIRS IR and SWC channels

A day–night difference in the brightness temperature difference BTD_{45} between VIRS channels 4 and 5 at low temperatures was reported by Inoue and Aonashi (2000). They reported daytime values of BTD_{45} as large as 2 K over thick cumulonimbus clouds, which usually act as blackbodies in both channels. Such differences are not obvious in any of the analyses presented above. To quantify this apparent diurnal variation, BTD_{45} was computed and averaged for each day and night during the first 8 months of 1998 using only those data having $L_{V4} < 3$ W m^{-2} μm^{-1} Sr^{-1} or $T_{V4} < 238$ K. The resulting time series in Fig. 10a shows that BTD_{45} averages 2.1 and 1.4 K during sunlight and darkness, respectively, yielding an average day–night difference of 0.7 K. The day–night difference in BTD_{45} appears to be somewhat cyclical reaching a maximum of 1.3 K during day 48 and a minimum of -0.1 K during day 159.

If not properly taken into account, solar heating cycles induced by the orbit can cause small variations in thermal channel calibrations (Trishchenko and Li 2001). The beta angle, which is the angle between the plane of the spacecraft orbit and the line that connects the centers of the Earth and the sun, is a parameter that would be related to such heating cycles. Figure 10b shows the time series of the day–night difference in BTD_{45} with the squared cosine of the *TRMM* beta angle. The beta angle varies rapidly due to the orbit's precession. Although they do not track each other exactly, the two quantities are obviously related. The value of R between them is 0.48 indicating that the precession of the orbit can account for about half of the variation in the day–night difference in BTD_{45}. Some of the variability is likely due to changes in the viewed scene.

The results in Fig. 10 confirm the report of Inoue and Aonashi (2000) and show how the day–night difference varies. However, it does not explain whether one or both of the channels vary from day to night. To examine this question further, the separate day and night correlations between VIRS and the various instruments are examined more closely assuming that none of the other instruments has a diurnal variation in the response of the IR and SWC channels. Table 7 summarizes the day–night differences in the VIRS temperatures computed from the mean daytime and nighttime regressions for a given satellite y,

$$\Delta T_{\rm dni} = T_{{\rm V}i}({\rm day}, y, T_y) - T_{{\rm V}i}({\rm night}, y, T_y), \quad (11)$$

for $T_y = 200$ and 300 K. At $T_y = 300$ K, there is minimal day–night difference in the linear fits for all three satellites in either channel. This result confirms that any day–night problem in the VIRS IR and SWC channels is confined to low temperatures. The differences at lower temperatures are consistent for all three satellites. The average values of $\Delta T_{\rm dn}$ are 1.1 and 0.3 K for the IR and SWC channels, respectively, at $T_y = 200$ K. This result suggests that the average BTD_{45} in the daytime at 200 K is $\sim$0.8 K greater than that at night, a temperature excess that is very close to the average from Fig. 10. The bulk of the difference is due to the IR diurnal changes. Because the VIRS–*GOES-8* correlations cover the longest time period and the *GOES-8* and VIRS filter functions are the most similar, it may be concluded that the values of $\Delta T_{\rm dn}$ from the *GOES-8*–VIRS are the most reliable of the three. Thus, if only the *GOES-8* results are considered, it would appear that the SWC channel has no diurnal cycle and the entire effect is due to variations in the VIRS IR channel.

Separate day–night regressions were also computed using the CERES WN and VIRS IR and SWC data over ocean with $T_{V4} < 238$ K for a typical day, day 126, when the mean BTD_{45} day–night difference was 0.8 K. During daylight hours,

$$L_{V4} = 1.1025 L_{WN} + 0.0080, \quad (12)$$

$$L_{V5} = 1.0680 L_{WN} + 0.1052. \quad (13)$$

At night,

$$L_{V4} = 1.1210 L_{WN} - 0.0503, \quad (14)$$

$$L_{V5} = 1.0603 L_{WN} + 0.1477. \quad (15)$$

These fits yield results consistent with those in Table 7.

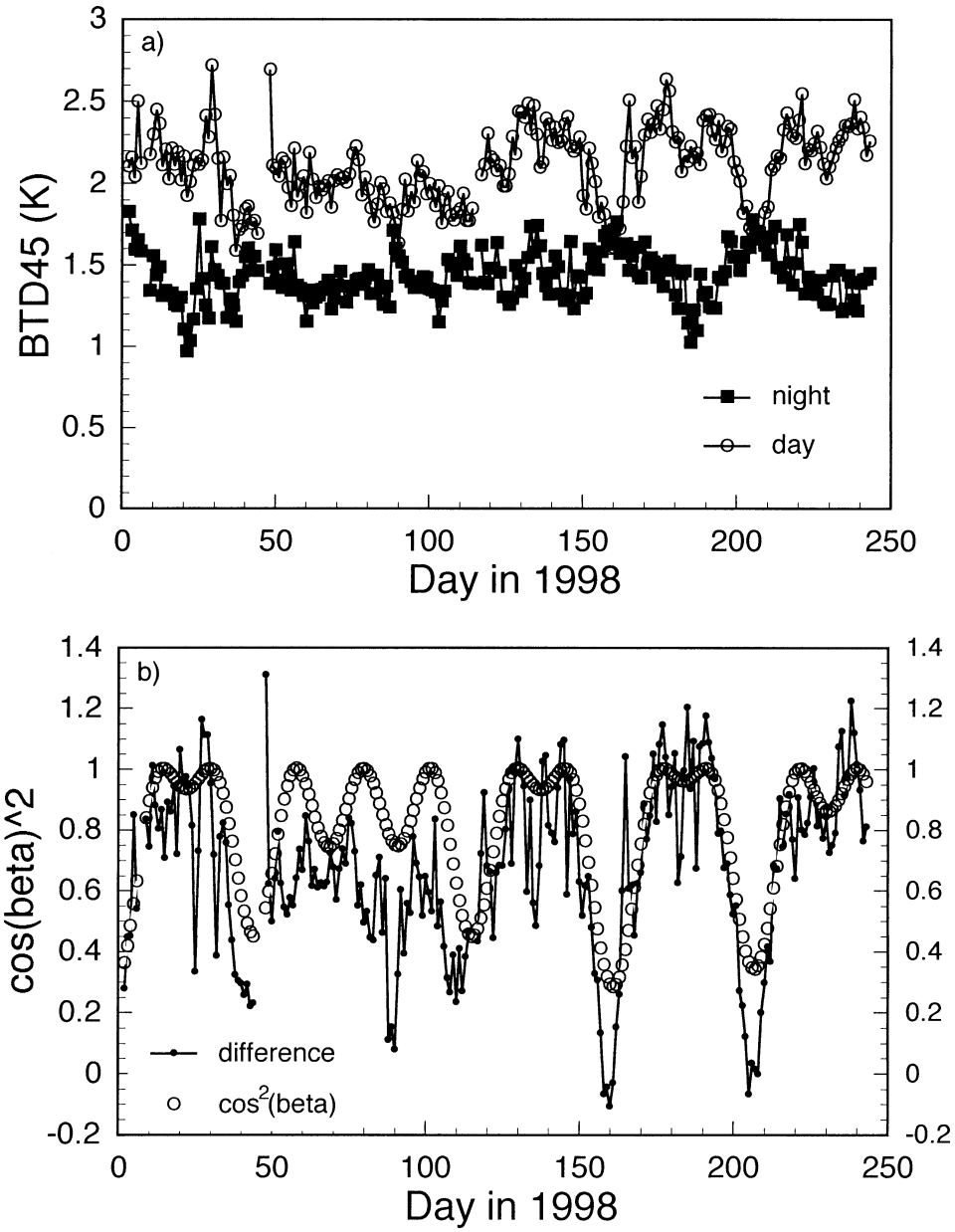

FIG. 10. Variation of (a) mean daily brightness temperature difference between VIRS channels 4 and 5 for $T_4 < 240$ K and (b) the day–night differences in BTD_{45} and the squared cosine of the *TRMM* beta angle.

At 200 K, BTD_{45} is 2.1 K greater during the day than at night. The day–night difference decreases with increasing temperature. At 238 K, it is only 0.5 K. Additionally, both channels yield day–night differences for the same value of L_{WN}. The difference is slightly larger for the IR channel. The CERES WN regression fits suggest that both channels change during the daytime; T_4 increases and T_5 decreases at low temperatures resulting in an increase of BTD_{45}. The results in Table 7 indicate, however, that both T_4 and T_5 increase during the day. Although these discrepancies preclude any firm conclusions about the variation in T_5, the increase in T_4 during the day is clearly evident.

From the results of Inoue and Aonashi (2000), it is likely that the nighttime VIRS temperatures are the most accurate. If the day–night difference is a result of solar heating of the blackbodies, then it is reasonable to assume that VIRS channel 3 is also affected. The effect cannot be determined in a similar manner, however, because the solar component in channel 3 eliminates the assumption, that daytime and nighttime conditions are the same on average, used for Table 7 and the CERES

TABLE 7. Day–night differences (K) in IR and SWC temperatures computed using mean linear fits between VIRS and other satellite data.

Channel	Temperature (K)	MODIS	*GOES-8*	*GMS-5*
IR	200	1.5	0.6	1.2
	300	−0.1	−0.2	−0.3
SWC	200	0.5	0.0	0.3
	300	−0.1	−0.2	−0.2

correlations. Users of the VIRS data should be aware of the potential for some day–night variations in the channel-3 calibration.

6. Conclusions

The comparisons between CERES and VIRS indicate that there is no discernible drift in the calibrations for any of the VIRS thermal channels through March 2000. Thus, the VIRS should be useful as a calibration reference for other satellite imagers. Any use of broadband data for detecting trends in narrowband data must take into account the seasonal variations of the viewed scenes. Apparently, changes in sea surface temperature and clouds can give rise to changes in the narrowband–broadband relationship. The comparisons with the CERES broadband data highlighted the potential for improving estimates of longwave flux from narrowband imagers. Because of its sensitivity to water vapor absorption, it was found that a split-window channel might be a better predictor of broadband longwave radiation than the infrared window channel that has been traditionally used to estimate the longwave flux. The CERES instruments have been operating for over 2 yr on the *Terra* satellite. The technique used here for monitoring the VIRS calibration can be applied more continuously to MODIS data and should be able to reveal any significant calibration trends.

Except for some significant discrepancies at low brightness temperatures, all of the thermal channels from the various satellites appear to be measuring temperatures to within 0.5 K or better. No trends were detected in any of the thermal channels on *GOES-8* or *GMS-5*. Some of the temperature differences between pairs of sensors are due to effects of the atmospheric constituents on the radiation within the various spectral bands defined by each sensor's filter function. The results highlight the need to explicitly account for the spectral differences between similar channels in future intercalibrations, especially as the accuracy requirements for remote sensing increase. Failure to account for small spectral differences can result in relative biases in parameters retrieved from the various sensors. Some of the differences, especially those at cold temperatures, may be due to small inaccuracies in the onboard blackbodies used to calibrate the thermal channels or to diurnal heating cycles that have not been taken into account. The differences at low temperatures are important and should be minimized as much as possible because they significantly impact remote sensing techniques that rely on small temperature differences. The diurnal cycle in the VIRS thermal channel calibrations could be minimized by developing a correction formulated in terms of the satellite–sun angle. These intercalibrations are continuing with a 1-month turnaround. Faster intercalibrations can be obtained on a daily basis. NG01 discuss these techniques in Part III of the paper.

Acknowledgments. This research was supported by the CERES Project through the NASA Earth Science Enterprise and by the Environmental Sciences Division of U.S. Department of Energy Interagency Agreement DE-AI02-97ER62341 through the ARM Program. The ATSR-2 data were provided by the ATSR Data Processing Laboratory, Rutherford Appleton Laboratory, Chilton, United Kingdom, with the assistance of Mr. Nigel Houghton under the sponsorship of the Natural Environment Research Council and the European Space Agency. Thanks to Vince Salomonson and William Barnes of the MODIS team for their assistance with the MODIS data and the NASA Langley Distributed Active Archive Center for supplying the CERES, MODIS, and VIRS data. The assistance of Cheng-Hsuan Lyu for his aid in deciphering the MODIS and VIRS calibration procedures is very much appreciated. The *GOES-8* and *GMS-5* data were acquired from the University of Wisconsin Space Science and Engineering Center.

REFERENCES

Barkstrom, B. R., E. F. Harrison, and R. B. Lee III, 1990: Earth Radiation Budget Experiment—Preliminary seasonal results. *Eos,* **71,** 297 and 304.

Barnes, R. A., W. L. Barnes, C.-H. Lyu, and J. L. Gales, 2000: An overview of the Visible and Infrared Scanner radiometric calibration algorithm. *J. Atmos. Oceanic Technol.,* **17,** 395–405.

Barnes, W. L., T. S. Pagano, and V. V. Salomonson, 1998: Prelaunch characteristics of the Moderate Resolution Imaging Spectroradiometer (MODIS) on EOS–AM1. *IEEE Trans. Geosci. Remote Sens.,* **36,** 1088–1100.

Brest, C. L., W. B. Rossow, and M. D. Roiter, 1997: Update of radiance calbrations for ISCCP. *J. Atmos. Oceanic Technol.,* **14,** 1091–1109.

Butler, J. J., and R. A. Barnes, 1998: Calibration strategy for the Earth Observing System (EOS)–AM1 platform. *IEEE Trans. Geosci. Remote Sens.,* **36,** 1056–1061.

Doelling, D. R., P. Minnis, D. A. Spangenberg, V. Chakrapani, A. Mahesh, F. P. J. Valero, and S. Pope, 2001: Cloud radiative forcing during FIRE ACE derived from AVHRR data. *J. Geophys. Res.,* **106,** 15 279–15 296.

Green, R. N., and B. A. Wielicki, 1995: Convolution of imager cloud properties with CERES footprint point spread function (subsystem 4.4). Clouds and the Earth's Radiant Energy System (CERES) algorithm theoretical basis document. Vol. 3, Cloud analyses and radiance inversions (subsystem 4). NASA Rep. 1376, 177–194.

Inoue, T., and K. Aonashi, 2000: A comparison of cloud and rainfall information from instantaneous visible and infrared scanner and precipitation radar observations over a frontal zone in East Asia during June 1998. *J. Appl. Meteor.,* **39,** 2292–2301.

Kratz, D. P., 1995: The correlated *k*-distribution technique as applied to the AVHRR channels. *J. Quant. Spectrosc. Radiat. Transfer,* **53,** 501–517.

Lee, R. B., III, and Coauthors, 1998: Prelaunch calibrations of the Clouds and Earth's Radiant Energy System (CERES) Tropical Rainfall Measuring Mission and Earth Observing System Morning (EOS–AM1) spacecraft thermistor bolometer sensors. *IEEE Trans. Geosci. Remote Sens.,* **36,** 1173–1185.

Lyu, C. H., R. A. Barnes, and W. L. Barnes, 2000: First results from the on-orbit calibrations of the Visible and Infrared Scanner for the Tropical Rainfall Measuring Mission. *J. Atmos. Oceanic Technol.,* **17,** 385–394.

Menzel, W. P., and J. F. W. Purdom, 1994: Introducing *GOES-I*: The first of a new generation of Geostationary Operational Environmental Satellites. *Bull. Amer. Meteor. Soc.,* **75,** 757–781.

Minnis, P., and E. F. Harrison, 1984: Diurnal variability of regional cloud and clear-sky radiative parameters derived from GOES data. Part III: November 1978 radiative parameters. *J. Climate Appl. Meteor.,* **23,** 1032–1052.

——, and W. L. Smith Jr., 1998: Cloud and radiative fields derived from *GOES-8* during SUCCESS and the ARM–UAV spring 1996 flight series. *Geophys. Res. Lett.,* **25,** 1113–1116.

——, D. F. Young, and E. F. Harrison, 1991: Examination of the relationship between infrared window radiance and the total outgoing longwave flux using satellite data. *J. Climate,* **4,** 1114–1133.

——, D. P. Garber, D. F. Young, R. F. Arduini, and Y. Takano, 1998: Parameterization of reflectance and effective emittance for satellite remote sensing of cloud properties. *J. Atmos. Sci.,* **55,** 3313–3339.

——, L. Nguyen, D. R. Doelling, D. F. Young, and D. P. Kratz, 2002: Rapid calibration of operational and research meteorological satellite imagers. Part I: Evaluation of research satellite visible channels as references. *J. Atmos. Oceanic Technol.,* **19,** 1233–1249.

Mutlow, C. T., M. J. Murray, D. L. Smith, P. D. Watts, and P. North, 1999: New data sets for climate change and land use studies are on track. *Eos,* **49,** 589 and 594.

Priestley, K. J., and Coauthors, 2000: Postlaunch radiometric validation of the Clouds and the Earth's Radiant Energy System (CERES) proto-flight model on the Tropical Rainfall Measuring Mission (TRMM) spacecraft through 1999. *J. Appl. Meteor.,* **39,** 2249–2258.

Smith, W. L., S. Ackerman, H. Revercomb, H. Huang, D. H. DeSlover, W. Feltz, L. Gumley, and A. Collard, 1998: Infrared spectral absorption of nearly invisible cirrus clouds. *Geophys. Res. Lett.,* **25,** 1137–1141.

Thomas, S., and Coauthors, 2000: On-orbit radiometric performance results of CERES instruments aboard Tropical Rainfall Measuring Mission (TRMM) and Earth Science Enterprise Terra spacecraft. *Proc. Fifth Pacific Ocean Remote Sensing Conf.,* Goa, India, Australian Bureau of Meteorology, 127–131.

Trishchenko, A., and Z. Li, 2001: A method for the correction of AVHRR onboard IR calibration in the event of short-term radiative contamination. *Int. J. Remote Sens.,* **22,** 3619–3624.

Weinreb, M., M. Jamison, N. Fulton, Y. Chen, J. X. Johnson, J. Brenner, C. Smith, and J. Baucom, 1997: Operational calibration of Geostationary Operational Environmental Satellite-8 and -9 imagers and sounders. *Appl. Opt.,* **36,** 6895–6904.

Wielicki, B. A., and Coauthors, 1998: Clouds and the Earth's Radiant Energy System (CERES): Algorithm overview. *IEEE Trans. Geosci. Remote Sens.,* **36,** 1127–1141.